# *Articles*

## Determination by Means of X-ray Absorption Spectroscopy and Transmission Electron Microscopy of the Local Structure of the 2D-Misfit Compound $[Sr(Fe_{0.77}Nb_{0.23})_{0.5}S_{1.5}]_{1.13}NbS_2$

Olivier Leynaud,† Maria Teresa Caldès, Catherine Guillot-Deudon, Guy Ouvrard, Alain Lafond, and Alain Meerschaut*

*Institut des Matériaux Jean Rouxel, Laboratoire de Chimie des Solides, UMR-CNRS 6502, 2 rue de la Houssinière, B.P. 32229, 44322 Nantes Cedex 03, France*

*Received March 24, 2003. Revised Manuscript Received July 15, 2003*

The $[Sr(Fe_{0.77}Nb_{0.23})_{0.5}S_{1.5}]_{1.13}NbS_2$ phase belongs to the 2D-misfit compounds family which are formed of two kinds of slabs labeled Q and H. The Q-part is a three-layer-thick slab, with the NaCl type structure, where external SrS planes enclose the inner (Fe,Nb)S plane. In a previous paper it was shown that there is a statistical distribution of the iron and sulfur atoms in the central layer of the Q-part. On the other hand, niobium atoms adopt an octahedral environment. To get a better description of this central layer, X-ray absorption and HREM studies were undertaken. EXAFS measurements clearly show that the environment of Fe atoms is less complex than that suggested from the structural determination. The existence of only one value for the Fe−S distance confirms the presence of $[FeS_4]$ tetrahedra as previously shown by the Mössbauer study. Both $[NbS_6]$ and $[FeS_4]$ polyhedra can arrange themselves in clusters. Electron diffraction and HREM studies reveal two new additional periodicities which can originate from the arrangement of these clusters. In this paper, a structural model is proposed in the large cell ($8a_Q \times 8b_Q \times c_Q$) which takes into account all these new experimental results. This model leads to the $[Fe/(Fe+Nb)]_Q$ ratio (0.75) very close to the value deduced from the microprobe analysis.

### Introduction

The 2D-misfit compounds $[((M,M')S)_{1.5}]_{1+x}NbS_2$, corresponding to the 1.5Q/1H alternated stacking type, have been recently reported for different couples of metal atoms such as M/M′ = Pb/Fe, Sr/Fe, Sr/Gd, $Eu^{II}/Eu^{III}$.[1−3] The presence of two kinds of atoms M/M′ results from the fact that the [(M,M′)S] subpart (Q-part) is a three-layer-thick slab where the M and M′ atoms are located on the external sides and in the central layer of this Q-sandwich, respectively. These two atoms have different oxidation states: $M^{2+}$ and $M'^{3+}$. If M′ is a small cation, such as $Fe^{3+}$, then M′ is statistically distributed on a four-split-position (in a tetrahedral coordination) around the central octahedral site which is partially occupied by Nb atoms. On the other hand, a large M′ cation (such as Eu) occupies a nonsplit position.

The magnetic measurements of the title compound have revealed a complex behavior likely related to the statistical occupancy of Fe atoms.[2] A disordered magnetic ion framework is thus resulting, with magnetic interactions of various intensities; it was not possible to establish, by a Curie−Weiss law fitting, the oxidation state of Fe because of the downward curvature of the $\chi^{-1}(T)$ curve. On the other hand, from the Mössbauer study a tetrahedral sulfur environment has been proposed with a valence close to +III for iron. This result needed to be confirmed by other techniques.

The absence of an answer about the Fe-oxidation state from magnetic measurements, correlated with the multiple combinations in occupancies of the split site for (Fe,Nb)/S atoms, convinced us to undertake an X-ray absorption spectroscopy study coupled with an electron microscopy study. The present paper reports the results of these studies and proposes a model of the distribution of the atoms in the central atomic layer of the Q-part.

### Structural Description

The structure of $[Sr(Fe_{0.77}Nb_{0.23})_{0.5}S_{1.5}]_{1.13}NbS_2$ was solved via the composite approach, and results of this study were recently published.[2] The composite character

* Corresponding author. Phone: +33-2-40-37-39-44. Fax: +33-2-40-37-39-95. E-mail: Alain.Meerschaut@cnrs-imn.fr.

† Present address: Max Planck Institute für Festkörperforschung, Heisenbergstrasse 1, D-70569 Stuttgart, Germany.

(1) Lafond, A.; Deudon, C.; Meerschaut, A.; Palvadeau, P.; Moëlo, Y.; Briggs, A. *J. Solid State Chem.* **1999**, *142*, 461−469.

(2) Leynaud, O.; Lafond, A.; Moëlo, Y.; Palvadeau, P.; Meerschaut, A. *J. Solid State Chem.* **2002**, *168*, 41−51.

(3) Cario, L.; Lafond, A.; Palvadeau, P.; Deudon, C.; Meerschaut, A. *J. Solid State Chem.* **1999**, *147*, 58−67.

10.1021/cm030300q CCC: $25.00 
Published on Web 09/13/2003

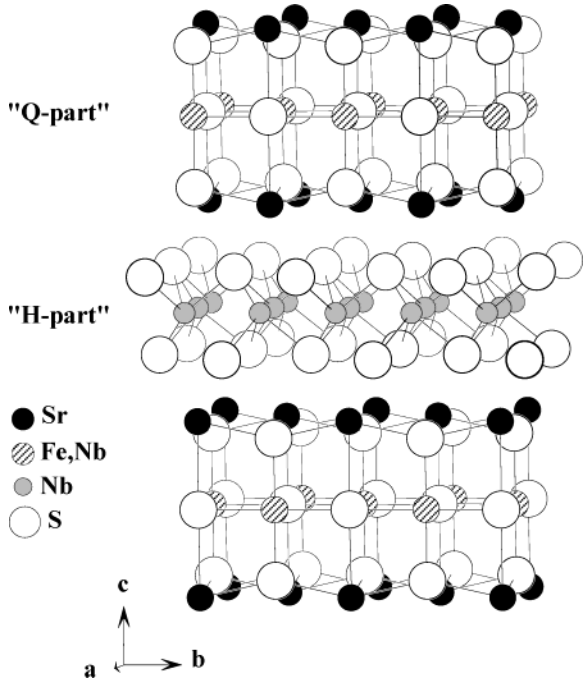


**Figure 1.** Stacking sequence structure of the 2D-misfit compound 1.5Q/1H. The Q-part is a three-layer pseudo-quadratic slab $[Sr_2(Fe,Nb)S_3]$ while the H-part is formed by a pseudohexagonal layered slab $[NbS_2]$.

of this 2D-compound is related to the stacking of the two Q and H structural units along [001], and its misfit characteristic is due to the noncommensurate in-plane periodicities $a_Q$ and $a_H$, namely $a_Q/a_H \approx \sqrt{3}$: this compound refers to the 1.5Q/1H alternating sequence (Figure 1). The Q-part (= (Sr, Fe)S) is related to an *F*-centered system ($c = 28.076$ Å), while the H-part is associated with a *C*-centered system ($c = 14.045$ Å). The title compound is isostructural with $[(EuS)_{1.5}]_{1.15}NbS_2$,[3] for which the structure was solved by the super-space approach ($G_s = Xm2m$ (α,0,0)). In this structure, the Q-part (EuS) consists of a three-layer-thick slab of NaCl structure type. $Eu^{2+}$ cations located on the exterior sides of this Q-part show a quite regular square pyramidal coordination, while the inner $Eu^{3+}$ cations show a distorted octahedral coordination. The H-part adopts the same structure as the binary $NbS_2$ compound itself, i.e., S atom planes sandwiching the central Nb plane in a trigonal prismatic coordination. In the Sr/Fe derivative $Sr^{2+}$ plays as $Eu^{2+}$ in the archetype compound, while Fe atoms should act as trivalent cations like $Eu^{3+}$, in connection with the charge-transfer mechanism.[4]

However, compared to the archetype $[(EuS)_{1.5}]_{1.15}NbS_2$, a structural difference is observed within the central layer of the Q-part. Indeed, in the Eu-derivative, Eu and S atoms are located on a special (4a) type position (0 *y* 0, with $y = 0$ for Eu and $y = 0.495$ for S) for the *Fm2m* space group (Figure 2a), while for the (Sr/Fe)-derivative (also *Fm2m* space group), both Fe and S atoms of the central layer are statistically occupying four-split positions (2 times 8c) around the central special position (4a) that is attributed to Nb only (Figure 2b). Thus, the site occupancy factors (sofs) are 0.227 for Nb (4a site), and 0.193 for Fe (8c site) atoms, which equals in total

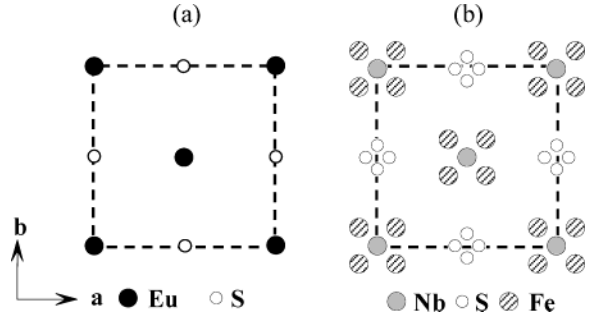


**Figure 2.** Detailed X-ray-diffraction structure of the central atomic layer in the Q-part for the 2D-misfit compound: (a) $[(EuS)_{1.5}]_{1.15}NbS_2$ (ref 3) = Eu/S; (b) $[Sr(Fe,Nb)_{0.5}S_{1.5}]_{1.13}NbS_2$ (ref 2) = Sr/Fe.

four atoms. This gives the structural formula $[Sr_1(Fe_{0.77},Nb_{0.23})_{0.5}S_{1.5}]_{1.13}NbS_2$, which is in very good agreement with results from the microprobe analysis: indeed, on the basis of S = 3.695 atoms (fixed by crystallographic data), one obtains the following chemical formulation $[Sr_{0.963}(Fe_{0.748},Nb_{0.230})_{0.5}S_{1.5}]_{1.13}NbS_2$. About the split positions that concern Fe as well as S atoms, it is interesting to notice that a similar feature (splitting) was also observed in the misfit layered cobaltite[5] $[Ca_2CoO_3][CoO_2]_{1.62}$ for Co and O atoms which are in the central plane of the Q part [= $Ca_2Co_3$].

## Experimental Section

**X-ray Absorption Spectroscopy (XAS).** XAS was done on the sample previously used for magnetic measurements;[2] all the crystals were selected one by one to get clean crystals without impurity deposits on their surfaces. This sample was carefully ground and homogenized to make a suitable thin pellet for XAS studies, after mixing it with an appropriate amount of cellulose.

X-ray absorption spectra were recorded on the experimental station D44 (LURE-DCI storage ring (1.85 GeV, average intensity 250 mA), Orsay, France). Data were collected in the transmission mode at the FeK edge on an XAS 4 spectrometer, using a double-crystal monochromator Si(111) for extended X-ray absorption fine structure (EXAFS) analysis and Si(311) for X-ray absorption near edge structure (XANES) analysis.

XANES spectra were recorded by steps of 1 eV with 1 s of accumulating time per point within the 7080−7100 and 7170−7230 eV energy ranges, whereas the step was 0.25 eV with an accumulating time of 2 s between 7100 and 7170 eV. EXAFS spectra were recorded between 7000 and 8200 eV with an accumulating time of 2 s for each point split by 2 eV steps.

The compounds used for comparison and as references in the EXAFS data treatment, namely $Cu_2FeGeS_4$,[6] $KFeS_2$,[7] and $FePS_3$,[8] contain respectively tetrahedral Fe(II), tetrahedral Fe(III), and octahedral Fe(II). The analysis of the EXAFS data was performed in a classical way using the WINXAS code.[9] The amplitude and phase functions have been extracted from the FEFF[10] tables.

**Transmission Electron Microscopy.** The samples were prepared by dispersing the powder in ethanol and depositing the solution on a holey carbon copper grid. The high-resolution transmission electron microscopy experiments were performed using a Hitachi H9000NAR (300kV) with a Scherzer resolution of 1.8 Å.

(4) Meerschaut, A.; Moelo, Y.; Cario, L.; Lafond, A.; Deudon, C. *Mol. Cryst. Liq. Cryst.* **2000**, *341*, 1−8.
(5) Lambert, S.; Leligny, H.; Grebille, D. *J. Solid State Chem.* **2001**, *160*, 322−331.
(6) Wintenberger, M. *Mater. Res. Bull.* **1979**, *14*, 1195−1202.
(7) Taft, C. A. *J. Phys.* **1977**, *38*, 1161−1162.
(8) Ouvrard, G.; Brec, R.; Rouxel, *J. Mater. Res. Bull.* **1985**, *20*, 1181−1189.
(9) Ressler, T. *J. Phys. IV* **1997**, C2−269.
(10) Rehr, J. J. *J. Appl. Phys.* **1993**, *32*, 8.

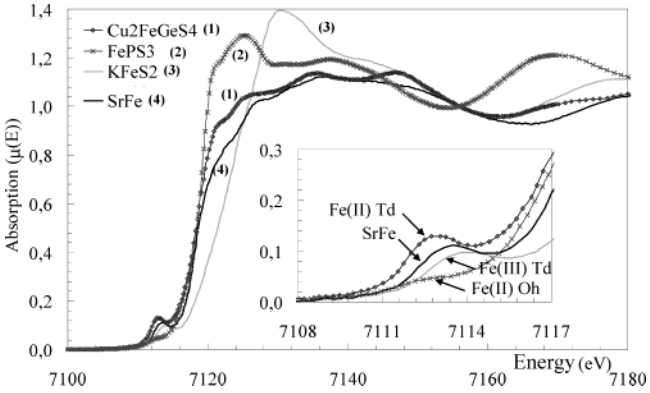


**Figure 3.** XANES spectra at Fe K-edge for some references and the compound Sr/Fe (strong solid line). Inset shows a zoom on the preedge part; Td = tetrahedral, Oh = octahedral.

## Results and Discussion

**X-ray Absorption Spectroscopy.** Although the structure of the compound Sr/Fe was successfully solved by X-ray diffraction study,[2] because of the long range order sensitivity of X-ray diffraction, a precise description of the atomic order within the central atomic plane of the Q-part could not be given. This plane was so far described by a statistical split of the iron and sulfur atoms; furthermore, the iron was assumed to be partially substituted by niobium. In consequence, our main goal was to determine the local order which arises in this material. The first step in this study is the use of XAS techniques at the Fe*K* absorption edge. XANES is useful to determine the local environment and to confirm the oxidation state of iron atoms. EXAFS studies can provide information on the number of neighbors and on the bond lengths around the absorbing Fe atom.

*XANES*. The absorption spectra of the three references and of the Sr/Fe compound are shown in Figure 3. Two main results are obtained from these data. First, the slope and the position of the main absorption edge of the Sr/Fe compound is very close to that of the references expressing a predominantly +II oxidation state for iron. The second important fact concerns the peak located just before the main absorption edge for Sr/Fe. This peak is the signature of a non centrosymmetric environment of the absorbing atom. For two of the reference compounds, iron atoms are tetrahedrally coordinated and present such a peak. This confirms the tetrahedral environment of the iron in Sr/Fe. But, at this step, the existence of an octahedral environment for some Fe cannot be completely excluded. A more definitive conclusion can be achieved by the use of the EXAFS technique.

*EXAFS*. Figure 4 shows the radial distribution functions for the Sr/Fe compound and for the three standards used as references in the data treatment.

The first peak observed for the Sr/Fe compound (see Figure 4) is almost identical to the one observed in $Cu_2FeGeS_4$ (Fe(II) in tetrahedral coordination). The sharpness of this peak is very surprising because of the great number of possible Fe−S distances from the X-ray diffraction model (in connection with the split positions of iron and sulfur atoms). The Fe coordination in the first shell has been fitted and the quality of the refinement can be checked on Figure 5 showing the EXAFS signals (solid line, calculated; circles, experimental).

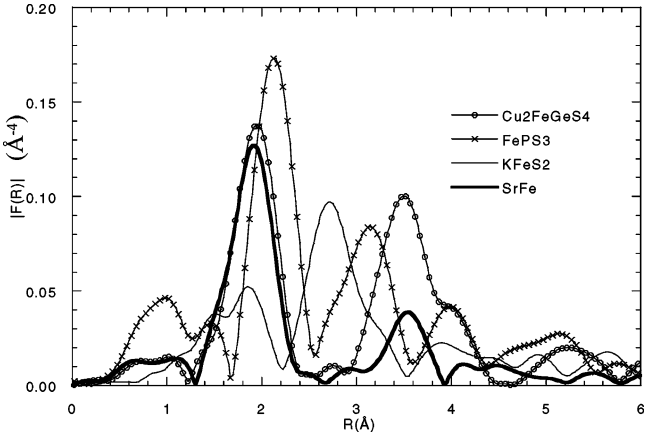


**Figure 4.** Radial distribution functions obtained from EXAFS spectra of each reference and of the Sr/Fe compound. For the latter compound, the narrow peak observed between 1.3 and 2.4 Å corresponds to a unique Fe−S distance in the first shell.

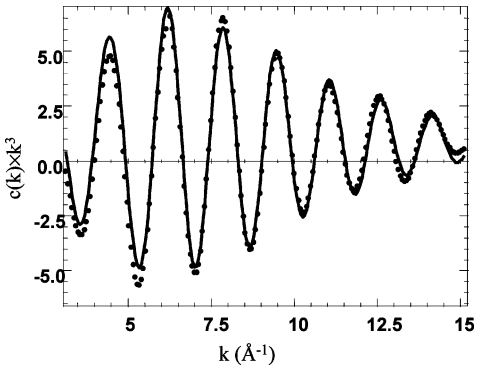


**Figure 5.** Comparison between the experimental (dotted line) and calculated (full line) Fourier transforms of the EXAFS spectra, corresponding to the first coordination shell.

The refinement of the first shell (between 1.3 and 2.4 Å; on Figure 4) leads to a coordination number $N = 3.8$ at 2.29 Å ($\sigma^2 = 0.0054$ Å$^2$). Attempts to introduce Fe−S distances at 2.5 Å, as expected for an octahedral environment, gave a coordination number of 0. These results exclude unambiguously the presence of iron in the octahedral site and then confirm that all Fe atoms are located in tetrahedral sites. Consequently, all niobium atoms present in the central atomic plane of the Q-part are supposed to be located in the octahedral position. EXAFS measurements at the niobium edge were done to confirm the octahedral coordination of Nb (as found from X-ray diffraction structure determination). However, no significant results could be obtained because of the low atomic fraction of Nb in the Q-part compared to that within the H-part, and a much-too-complex Nb mean environment.

Another remarkable observation for this shell is the existence of only one value for the Fe−S distance. The refinement of this distance leads to a value of 2.29 Å. Among all the possible Fe−S distances, the refined value is very close to the distance (2.34 Å) indicated on Figure 6a. This environment confirms the existence of tetrahedra [$FeS_4$] as previously suggested by the crystal structure determination. Because of the complex environment of iron (distances, nature, and number of second neighbors) the second coordination shell has not been fitted.

So, from the EXAFS results, the situation within the central atomic layer of the Q-part is very simple. Indeed,

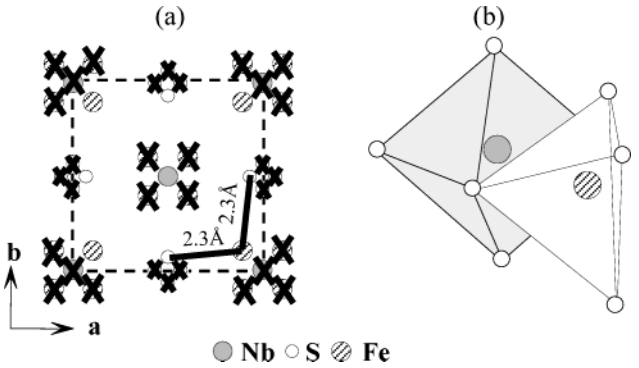


**Figure 6.** (a) Splitting of the atomic sites within the central plane of the Q-part for the compound Sr/Fe. Fe atoms are located in tetrahedral sites while Nb atoms stay in an octahedral position. Crosses indicate positions of the rejected atoms. The value of the Fe−S distance (2.34 Å) comes from the structure determination. (b) "Clusters" can be formed using 4 [$FeS_4$] tetrahedra and an [$NbS_6$] octahedron; only one tetrahedron is shown.

the nature of the atom on the (Nb,Fe) site implicates an unambiguous choice for the nature and the position of the neighbors (Figure 6a). By this way, the arrangement of the atoms should present [Nb,Fe] clusters, formed by [$FeS_4$] tetrahedra surrounding a [$NbS_6$] octahedron (Figure 6b).

To check if these clusters show a local order in this material, transmission electron microscopy experiments were undertaken.

**Transmission Electron Microscopy.** Selection area electron diffraction pattern (SAED) of a single crystal (Figure 7a) along the [001] zone axis reveals the main reflections of the two sublattices (Q and H) and the satellite reflections resulting from the mutual interaction between the Q- and H-parts, i.e., from displacive modulation within the two composite parts, as described above (Figure 7b). Most of the observed reflections have been indexed according to the four-integer notation ($h_Q$, $k$, $l$, $h_H$).[11] Note that the (1, 1, 1, 0) and (3, 1, 1, 0) reflections come from the first-order Laue zone (FOLZ) due to the large *c*-parameter and the weak thickness of the crystal. However, the spots on the dotted circle in Figure 7a cannot be indexed. In fact, two sets of reflections oriented at 30° from each other can be described (see dotted and full circles in Figure 7a). These two sets can be attributed to two orientational variants. On Figure 8, the [001] HREM image, corresponding to a part of a single crystal studied by SAED, is shown. The experimental contrast can be described as a pseudo-square symmetry arrangement of bright dots. Note that somewhat additional diffuse dark lines with a periodicity of 8.3 Å are visible in the plane (110). To get a better contrast, the image was filtered with the CRISP program[12] taking into account all the reflections observed in the Fourier function transform (FFT) pattern (Figure 9), including the extra spots on the circle (Figure 7a). Note that only one of the two sublattices described above is visible. The intensity of the contrast is modulated along the a-misfit direction. Indeed, four bright dots

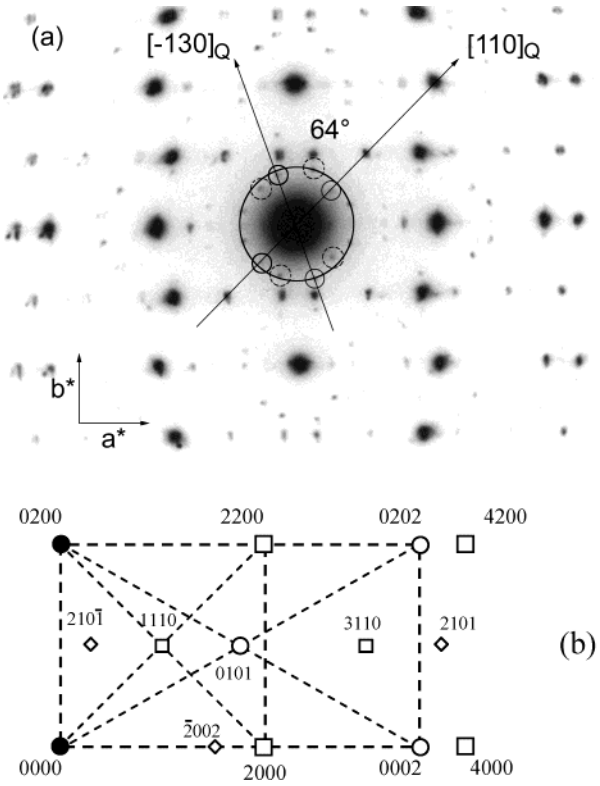


**Figure 7.** (a) Electron diffraction pattern of the SrFe phase along the [001] zone axis. The 2-D monoclinic cell is indicated by white arrows. (b) Schematic representation of the [001] electron diffraction pattern. The diffraction spots are indexed according to a four-integer notation ($h_Q$, $k$, $l$, $h_H$) except for the spots on the circle which cannot be indexed.

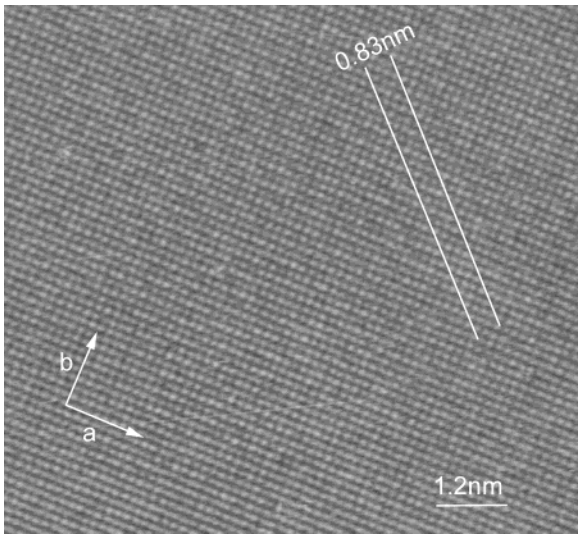


**Figure 8.** [001] HREM image of the title phase. The additional periodicity of 8.3 Å in the [110] direction is indicated.

alternate with three gray ones in this direction. This sequence is not the same all over the crystal. Furthermore, along the [010] direction, the modulation of the intensity of the rows is in anti-phase. To analyze the observed contrast a theoretical image was calculated using the multislices method (Mac Tempas program[13]). The real structure of this incommensurate compound should be described using the superspace approach.

(11) van Smaalen, S. *Mater. Sci. Forum* **1992**, *100&101*, 173−222.
(12) Hovmöller, S. CRISP − Crystallographic Image Processing on a Personal Computer. *Ultramicroscopy* **1992**, *40*, 121−135. Zou, X. D.; Sukharev, Y.; Hovmöller, S. *Ultramicroscopy* **1993**, *49*, 147−158. Zou, X. D.; Sukharev, Y.; Hovmöller, S. *Ultramicroscopy* **1993**, *52*, 436−444. Zou, X. D. Ph.D. Thesis. *Stockholm University Chem. Commun.* **1995**, 5.

(13) Kilaas, R. *Mac Tempas Program v1.70*; University of California: Berkeley, CA.

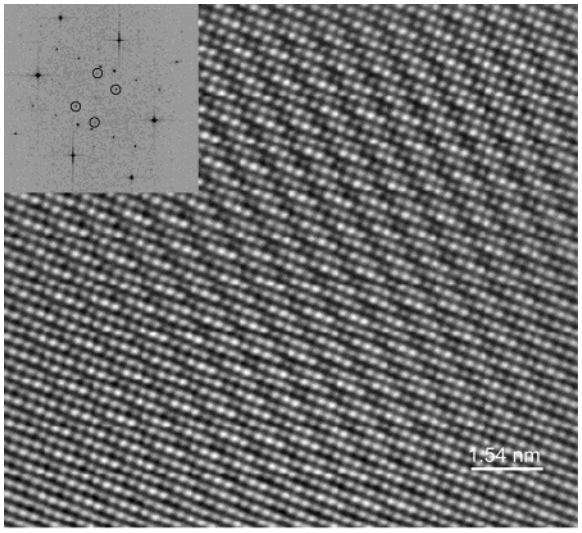


**Figure 9.** Inverse Fourier transform using both main reflections and extra spots. The inset shows the corresponding Fourier transform of the crystal.

However, this formalism is not available with the Mac Tempas program. Because the $a_Q/a_H$ ratio is close to 7:4, a commensurate supercell with $a = 4a_Q = 7a_H = 23.56$ Å, $b = 5.83$ Å, and $c = 28.08$ Å was considered. This first model was built without taking into account the statistical distribution of the atoms in the central atomic layer of the Q-part. A calculated through-focus series for a crystal thickness of 10 nm was done. The best fit between experimental and calculated images was obtained for a defocus value of −15 nm (Figure 10). For this defocus value the projected potential maxima appears as dark contrast. To analyze the HREM contrast atomic positions are overlaid in Figure 10b. Note that only the projection of S atoms of the H slab, which are located in the middle of the four atomic columns of the 1.5Q slab, are imaged as bright dots. However, the thin dark lines, with a periodicity of 8.3 Å, were not reproduced by this model. These dark lines could indicate an ordering of the atoms in the central atomic layer of the Q-part, which could explain the presence of the extra spots in Figure 7a.

**Model Construction.** At this stage of the work, the structural model has to be improved by taking into account the following experimental results.

(a) The presence of two sets of extra spots on the SAED pattern. One of the two sets of extra spots leads to new periodicities along [110] and [−130] of the Q-subsystem drawing an angle of 64°. So, a 2D-monoclinic cell was determined with the following parameters: $a_{mono} = 9.3$ Å, $c_{mono} = 8.45$ Å, and $\beta = 116°$. Unfortunately, this monoclinic cell does not allow the description of the whole structure in a commensurate supercell.

(b) The dark lines on the HREM image (periodicity 8.3 Å).

(c) Results of the EXAFS study indicating that Fe atoms are only on the tetrahedral sites, whereas Nb atoms are in octahedral sites with $d(Fe-S) \approx 2.34$ Å, leading to [Nb,Fe] clusters.

(d) The $Fe/(Fe + Nb_Q)$ ratio (0.76) deduced from the microprobe analysis. According to the arrangement of the [Nb,Fe] clusters, one gets different values for this ratio.

(e) Finally, the description of the atomic positions (Fe, Nb, S) in the central layer of the Q-part has to be done in a supercell $a = n \times 4a_Q$ due to the ratio $a_Q/a_H = 7:4$.

Under these considerations, a model with a supercell of $8a_Q \times 8b_Q \times c_Q$ containing 2880 atoms is proposed (Figure 11). This model shows two types of clusters: $[NbFe_4S_4]$ and $[NbFe_2S_4]$. These clusters are both built up from $[FeS_4]$ tetrahedra, with the same distances Fe−S, surrounding one $[NbS_6]$ octahedron. The arrangement of these clusters leads to $Fe/(Fe + Nb_Q) = 0.75$.

A theoretical electron diffraction pattern was calculated from this model (Figure 12); it fits quite well with the experimental one (Figure 7a). Indeed, main reflec-

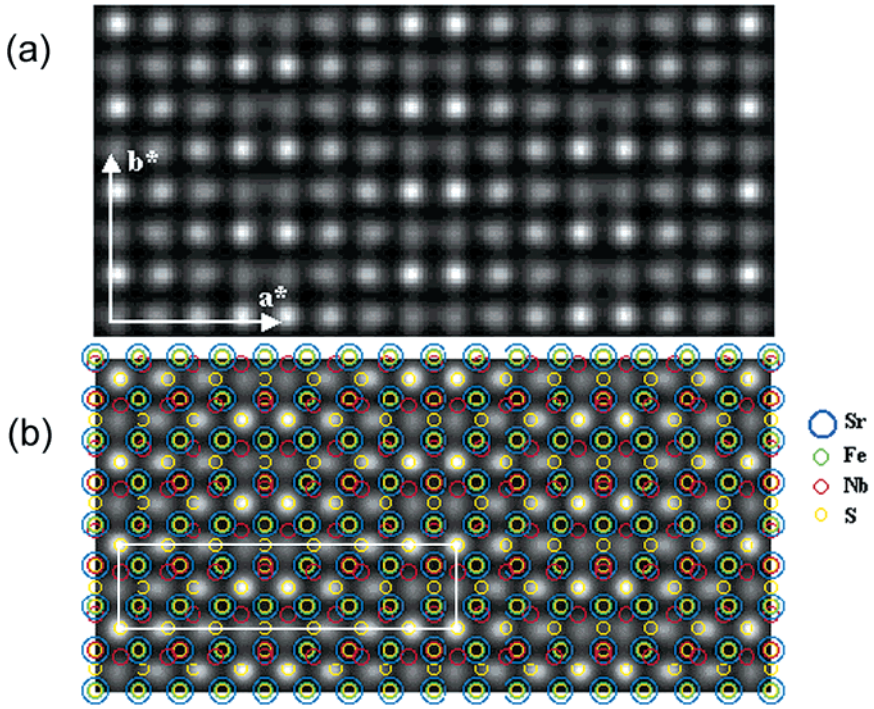


**Figure 10.** (a) Calculated image using a commensurate cell with $a = 4a_Q = 7a_H = 23.56$ Å, $b = 5.83$ Å, $c = 28.8$ Å. (b) Atomic positions are overlaid on the calculated image.

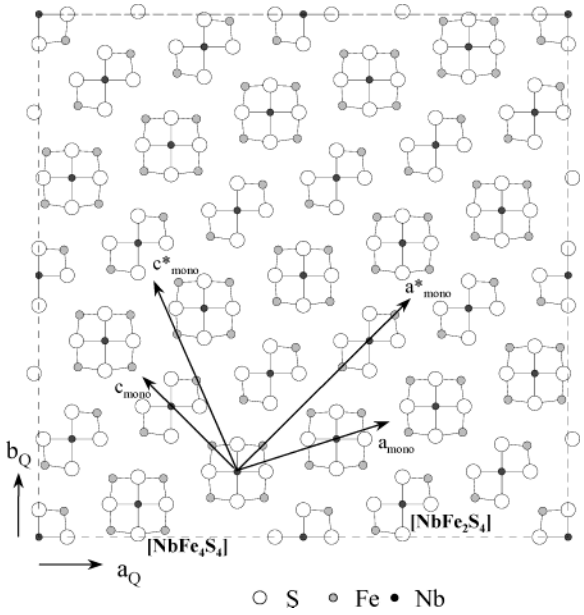


**Figure 11.** Model of the atomic positions (Fe, Nb, S) in the central layer of the Q-part showing the two types of clusters ($[NbFe_4S_4]$ and $[NbFe_2S_4]$) in the supercell of $8a_Q \times 8\ b_Q \times c_Q$. The monoclinic cell deduced from the SAED extra spots is drawn in solid line.

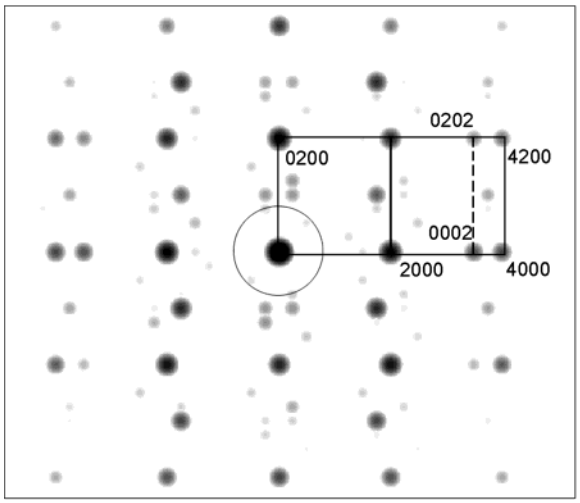


**Figure 12.** Calculated diffraction pattern using the model presented in Figure 11.

tions corresponding to the Q and H parts, and the satellite reflections, are well simulated. Moreover, the extra spots leading to new periodicities in the Q-sublattice are quite well reproduced. Note that in the SAED experimental pattern two sets of these extra reflections are visible; they correspond to two orientational variants. However, some weak reflections calculated by our model are not observed in the experimental pattern. This fact is not surprising because the atomic positions are idealized and are not refined because of the great number of atoms. So, the calculated amplitudes are probably not always relevant. Note that the satellite reflections corresponding to the new superstructure are much weaker than all the other ones. So, to better visualize the influence of the atoms order on the image contrast a filtered image was calculated. To

(14) Caldès, M. T.; Deniard, P.; Zou, X. D.; Marchand, R.; Diot, N.; Brec, R. *Micron* **2001**, *32*, 497−507.

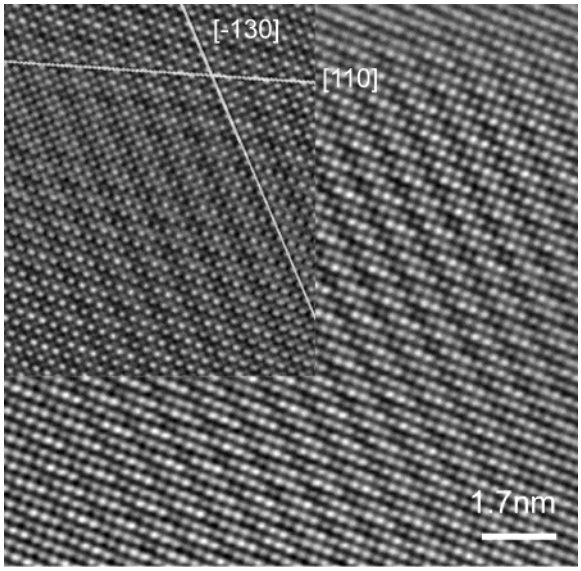


**Figure 13.** Inverse Fourier transform of the experimental image (a) and the calculated image (b) for a crystal thickness of 10 nm and a defocus value of −15 nm. Both inverses' FT were calculated with the amplitudes of the main reflections weighted down to 30%.

enhance the contribution of the cation ordering to the image contrast, the $(FFT)^{-1}$ image was calculating using the supercell model, with the amplitudes of the main reflections weighted down to 30%.[14] The same filtered conditions were applied for the experimental image (Figure 8).

In Figure 13, both experimental and calculated filtered images for a crystal thickness of 10 nm and a defocus value of −15 nm are presented. The calculated image using the new model reproduces the diffuse dark lines with a periodicity of 8.3 Å observed on the experimental image (Figure 8). The fit between both images is quite good. However, the additional diffuse lines observed along $a_{mono}$ were not observed on the original image. Note that these diffuse lines were not observed on the first calculated image using the supercell model. They appeared only when the amplitudes of main reflections were weighted down to 30%, as one can expect from the weak intensity of the satellite reflections.

The agreement between calculated and experimental images suggests that the model described above could be valid.

## Conclusion

A better description of the structure of $[Sr(Fe_{0.77}Nb_{0.23})_{0.5}S_{1.5}]_{1.13}NbS_2$ was achieved by the use of X-ray absorption spectroscopy and transmission electron microscopy. An order within the central atomic layer in the Q-part has been evidenced and a cluster model is proposed. This model takes into account all the experimental results (microprobe analysis, TEM observations, and EXAFS results). It is probably a good description of the atoms ordering in the central atomic layer of the Q-part which was not observed from the X-ray diffraction study.

Other models could be envisioned but it seems impossible to propose another one which fits the experimental results without using a larger cell.

CM030300Q